

Article

Preliminary Study on Optimization of a Geothermal Heating System Coupled with Energy Storage for Office Building Heating in North China

Yapeng Ren ^{1,2}, Xinli Lu ^{1,2,*} , Wei Zhang ^{1,2}, Jiaqi Zhang ^{1,2} , Jiali Liu ^{1,2}, Feng Ma ³, Zhiwei Cui ^{1,2}, Hao Yu ^{1,2}, Tianji Zhu ^{1,2} and Yalin Zhang ^{1,2}

¹ Tianjin Geothermal Research and Training Center, College of Mechanical Engineering, Tianjin University, Tianjin 300350, China

² Key Laboratory of Efficient Utilization of Low and Medium Grade Energy, MOE, College of Mechanical Engineering, Tianjin University, Tianjin 300350, China

³ Institute of Hydrogeology and Environmental Geology, Chinese Academy of Geological Sciences, Shijiazhuang 050061, China

* Correspondence: xinli.lu@tju.edu.cn; Tel.: +86-185-2297-2804



Citation: Ren, Y.; Lu, X.; Zhang, W.; Zhang, J.; Liu, J.; Ma, F.; Cui, Z.; Yu, H.; Zhu, T.; Zhang, Y. Preliminary Study on Optimization of a Geothermal Heating System Coupled with Energy Storage for Office Building Heating in North China. *Energies* **2022**, *15*, 8947. <https://doi.org/10.3390/en15238947>

Academic Editors: Xiangfei Kong and Tailu Li

Received: 16 October 2022

Accepted: 24 November 2022

Published: 26 November 2022

Publisher's Note: MDPI stays neutral with regard to jurisdictional claims in published maps and institutional affiliations.



Copyright: © 2022 by the authors. Licensee MDPI, Basel, Switzerland. This article is an open access article distributed under the terms and conditions of the Creative Commons Attribution (CC BY) license (<https://creativecommons.org/licenses/by/4.0/>).

Abstract: Geothermal heating is considered to be one of the low-carbon-energy technologies for building heating. Aiming at the problem that the operating cost and investment cost of geothermal heating systems are still high, the conventional geothermal heating system coupled with energy storage for office building heating is studied in this paper. Four operational strategy models of the coupled system are established based on time-of-use electricity prices. A genetic algorithm is used to find the optimal value of each decision variable using minimization of levelized cost of heat (LCOH) as the objective function. The influences of electricity and equipment prices on the optimal values of the decision variables are discussed. Four operation strategies are investigated. If only operating cost is considered in the optimization, comparison shows that the best operation strategy is the one giving high priority to use the energy storage tank for heating during the peak electricity period. However, if the investment cost is further considered in the optimization, the best operation strategy is the one using the energy storage tank for heat load peak-regulating. In addition, based on the minimization of LCOH, an optimal energy storage ratio is found for each scenario, and suitable conditions of using energy storage tank are discussed. The geothermal heating system coupled with energy storage can have a good performance when the peak-valley electricity price difference is higher than CNY 0.566/kW·h (USD 0.0847/kW·h)⁺ or the energy storage tank price is lower than CNY 900/m³ (USD 134.64/m³). The results obtained from this study prove that the cost of geothermal heating systems can be effectively reduced by choosing an optimal operation strategy and using an energy storage device with an optimal energy storage ratio.

Keywords: optimization; geothermal heating system; energy storage; operation strategy; time-of-use electricity prices; levelized cost of heat

1. Introduction

1.1. Background

With the continuous progress of science and technology, the energy consumption in the building sector accounts for a significant share of global energy consumption, especially in developed countries where it can account for one-fifth to two-fifths. In the building sector, heating, ventilation, and air conditioning (HVAC) systems are the largest source of energy demand, accounting for 50% of the sector's energy consumption and 10–20% of total energy consumption in developed countries [1]. In China, building energy consumption also accounts for an important part of the total energy consumption. According to statistics, in 2018, energy consumption of buildings (such as heating, refrigeration, ventilation, air

conditioning, etc.) accounted for 21.7% of the total energy consumption in China, and carbon emissions accounted for 21.9% of the total energy emissions in China. It is expected that building energy consumption will surpass other energy consumption and rank first in the total energy consumption by 2030 [2,3]. Therefore, strengthening the use of renewable energy in buildings plays an important role in reducing greenhouse gas emissions and mitigating climate change. Geothermal energy is a clean, sustainable, and large-reserve renewable energy. It is produced and used in a way consistent with the wellbeing of future generations [4], and is widely used in heating [5] and for other needs [6,7]. At the same time, with the development of geothermal energy technology and the formulation of geothermal heating planning, geothermal heating has great development potential in the coming decades [8]. Exploration of an efficient and feasible geothermal heating system and heating scheme is the basis and key for the wide application of geothermal heating.

Recently, The Ministry of Housing and Urban–Rural Development of the People’s Republic of China issued a national standard. It is clearly stipulated in the specification that the temperature of water entering the geothermal well should not exceed 20 °C when developing geothermal energy for heating [9]. The requirements of the code are conducive to the full use of geothermal energy resources and make geothermal energy combined with heat pump heating inevitable. As a heat pump is used in the heating system, it needs to consume electricity during daytime heating, which will increase the peak load of the power grid and may adversely affect the load efficiency of public power facilities and power grid [10]. In addition, the characteristic of high electricity price during the day will cause higher operating cost of the system. All these have posed challenges to the application and promotion of geothermal energy. Therefore, the heating system needs an effective operation strategy to stabilize power demand and reduce peak electricity consumption [11]. At the same time, a smart heating operation strategy will also reduce the cost and thus achieve the promotion of geothermal energy heating systems.

1.2. Literature Review

Many studies on geothermal heating combined with heat pump utilization have been carried out. The concept of a “ground source heat pump (GSHP)” was first proposed by Zoelly et al. (1912) [12]. Because GSHP systems use geothermal energy to replace fossil fuel consumption, air quality can be improved. Meghann Smith et al. noted that the incremental costs associated with GSHP compared to other HVAC technologies are due to increased drilling costs [13]. However, when GSHP systems are designed correctly, initial costs can be recovered in the first 5 to 10 years of the total 20–25-year life of the system through efficiency savings [14,15]. Urchueguía et al. [16] compared and analyzed the operation of a GSHP system and an air source heat pump system in an office building in Spain. The results showed that the coefficient of performance (COP) of the GSHP system was higher than that of the air source heat pump system in both heating and cooling seasons. Spitler et al. [17] analyzed a GSHP system in a new student services building at Stockholm University, Sweden. The results showed that coefficient of performance can reach 3.7 ± 0.2 in the heating season. Michopoulos et al. [18,19] studied the basic parameters and energy flows of a GSHP system for a public building in the Thessaloniki area in 2007, and calculated the energy demand of a typical one-family house in the area in 2009. Both results showed that the renewable energy system with a ground heat exchanger had greater energy saving than the conventional system. Xu et al. [20] compared GSHP heating with boiler heating in Beijing residential buildings, and the results showed that GSHP had a large energy saving value in the whole lifecycle, and with the decrease of the ratio of coal to electricity, the energy saving contribution value of the heat pump will be more significant. Younes et al. [21] analyzed the ground heat exchanger in the GSHP system, and concluded that parameters such as inlet temperature and circulating fluid flowrate were important factors affecting the system’s performance. Martinopoulos et al. [22] compared conventional heating systems and found that GSHPs had lower costs after analyzing the operating costs for households in European Union countries. D’Agostino et al. [23–25] studied a system in which an earth-

to-air heat exchanger was placed upstream of an air handling unit. By optimizing the heat exchanger, they found that using an earth-to-air heat exchanger could significantly reduce the total thermal power. In addition, with the Chinese government's efforts to develop geothermal energy, the medium and deep geothermal heat pump (MD-GHP) system has gradually been used in China since 2005. The MD-GHP system has the advantages of small formation pollution, high COP, and easy implementation, and has good application prospects in the field of district heating [26]. However, more research on the MD-GHP focuses on the simulation of ground heat recovery, and there are still deficiencies in the overall heating system optimization.

Energy storage is a good choice to solve the problems of high peak load of power grid and high operating cost caused by using heat pumps. At present, some scholars have studied the heat pump heating system with the use of a water tank. Wangsik et al. [27] established a heat pump heating system with a heat storage device, and discussed the influence of two operation strategies, the heat storage priority method and the heat pump priority method, under the condition of fixed water tank size. Brecht Baeten et al. [11] proposed a model-predictive control strategy for heat pump heat storage and heating, and based on a simulation model, studied the influence of space heating heat storage tank size under different control settings on system load duration and user cost. Alexander Floss et al. [28] discussed how to improve the efficiency of a heat pump system by optimizing different integration modes of heat pump and energy storage device. Jens Glembin et al. [29] studied the operation efficiency of heat pump system coupled energy storage and proposed some problems that should be considered in the design of a composite system. In addition, some scholars studied the application of a geothermal heat pump system coupled with energy storage. Lv et al. [30] found that the combined energy system composed of ground source heat pump system and heat storage system can save more than one-third of the operating cost compared with the conventional ground source heat pump system. Qi et al. [31] studied a water storage system for 67,000 square meters of commercial buildings in Beijing, China. They concluded that the investment and the operating costs were reduced by 11% and 13%, respectively, compared with the conventional GSHP system.

Some literature reports show that geothermal energy combined with a heat pump heating system can provide higher performance coefficient, and the introduction of energy storage devices can achieve lower operating cost. This shows that it is feasible to apply thermal energy storage (TES) to a geothermal heat pump heating system based on the characteristics of peak-valley electricity prices, and it will not reduce the efficiency of heat storage system as do air source heat pumps at night when the electricity price is low [32]. Therefore, load redistribution can be better realized.

Most previous studies focused on the system of ground source heat pump combined with energy storage device. There are few studies on the heating of the cascade utilization of medium and deep geothermal energy coupled with energy storage devices, and the research on the heating strategy and system design optimization seem weak.

Therefore, it is necessary to carry out an investigation of a medium and deep geothermal heating system coupled with energy storage for office building heating. In this study, we propose such a coupled system with consideration of different scenarios. The aim of this study is to obtain the optimal system parameters and the optimal operation strategy. The results obtained in this study show that the proposed system is more applicable when peak-valley electricity price difference and water tank price meet certain conditions. The results obtained in this study are useful for the design of a geothermal heating system coupled with energy storage.

The remainder of this paper is organized as follows. In Section 2, three models (system model, operation model, and optimization model) are described in detail, including system layout, equipment types, operation modes and strategies, decision variables, and objective function. In Section 3, optimization of the decision variables of 10 different scenarios is carried out, the simulation results are analyzed, and the sensitivity analysis in terms of the

energy storage ratio is also conducted and discussed. In Section 4, the main findings of this study are concluded.

2. Model Description

The overall investigation procedure of this study is shown in Figure 1. Firstly, the layout of the coupled heating system is determined, based on which the system model is established. Then, the decision variables and objective function are chosen according to the operation characteristics of the system. After that, the optimal value of each decision variable is determined using minimization of levelized cost of heat (LCOH) as an objective function. In this study, a genetic algorithm is used to find the optimum values of the decision variables. The traditional genetic algorithm was improved by adjusting the degree of crossover and mutation probability in the late iteration to improve the efficiency of searching and alleviate the problem of falling into local optimal solution. Detailed descriptions of each part of the research model are given in the following sections.

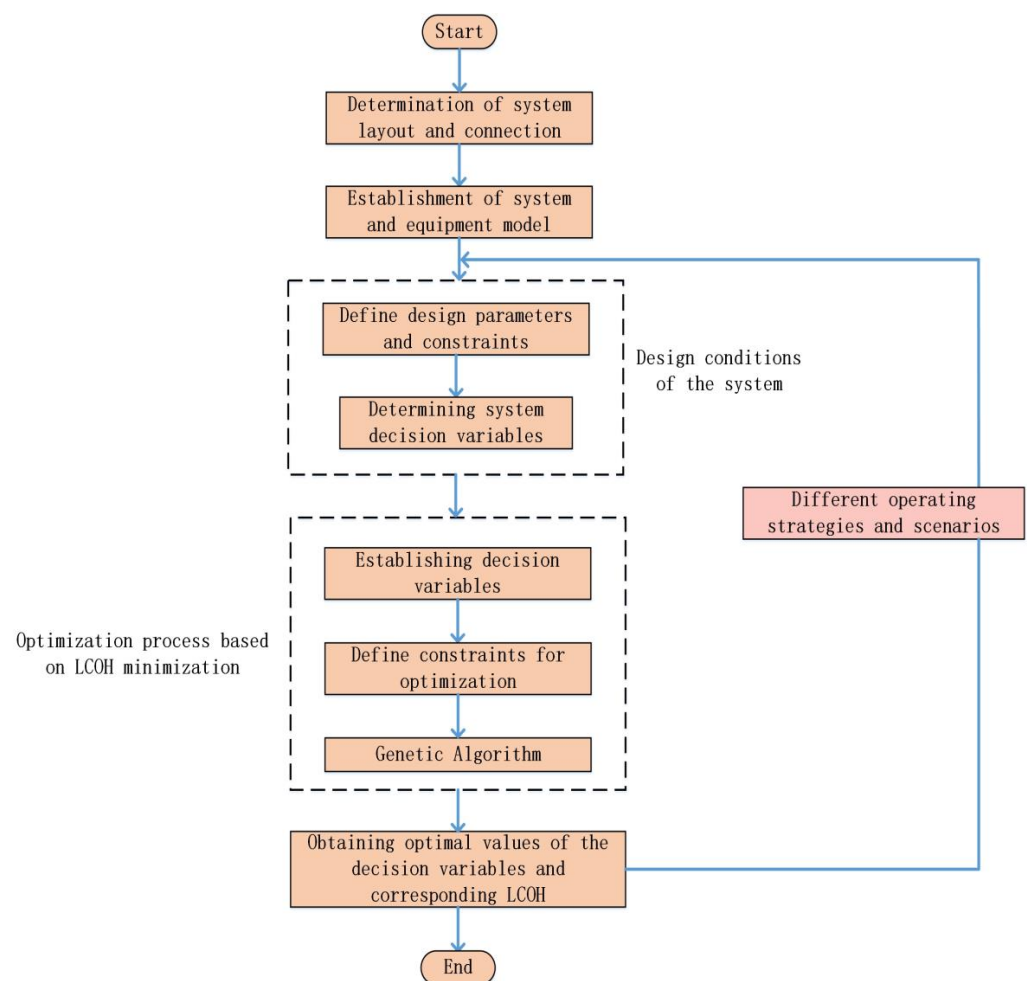


Figure 1. Investigation procedure of the study.

2.1. System Model

Figure 2 shows the energy storage–geothermal coupled heating system. Red, yellow, and blue in the figure indicate the temperature from high to low. V1 to V11 represent 11 valves. P1 to P4 represent the four water pumps. T1 to T13 represent the 13 temperature measurement locations. In this system, the high-temperature geothermal water from the production well flows through the Heat Exchanger 1 (high temperature) and the Heat Exchanger 2 (low temperature) to complete the two-stage heat transfer. After heat exchange in the Heat Exchanger 2, the heat of the circulating water driven by P3 is extracted by the

evaporator (e–f–g) and flows through the compressor (g–a), which is driven by electricity. The working fluid (with higher pressure and temperature) at the outlet of the compressor then enters the condenser, in which the heat energy is released (a–b–c–d) and transferred to the heating water at the building side. After that, the working fluid passes through an expansion valve (d–e), with lower pressure and temperature at the outlet of the valve. Then, the working fluid flows into the evaporator and another cycle starts again. The heat pump model described below is based on this heat pump cycle.

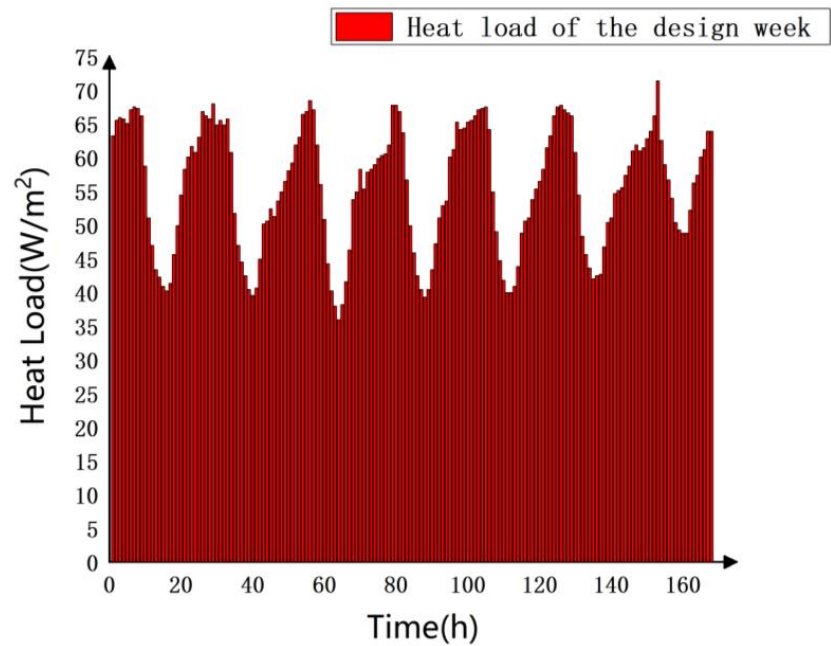


Figure 3. Heating load of the design week (7 consecutive days).

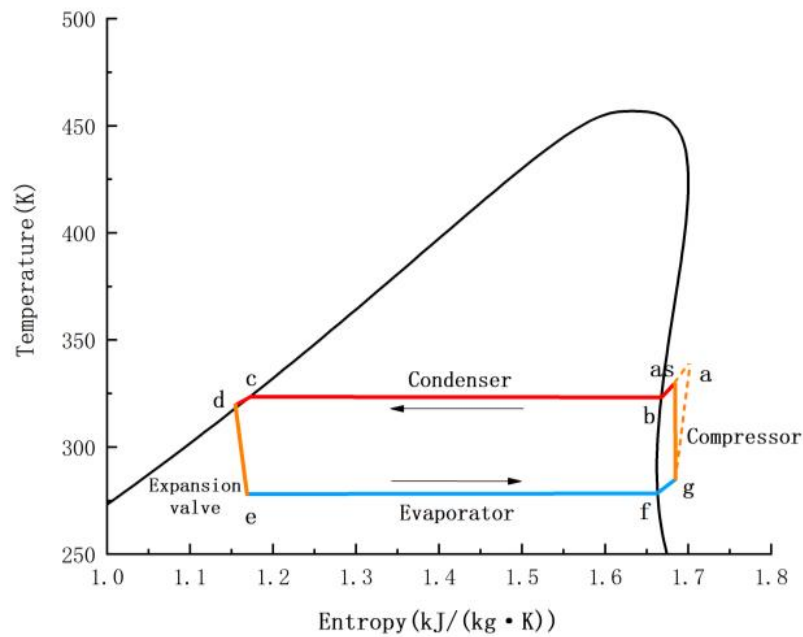


Figure 4. T–S diagram of the heat pump cycle (working fluid: R123).

The heat exchange rate in the evaporator:

$$Q_{eva}^{hp} = \dot{m}_{wf, hp}(h_g - h_e) = \dot{m}_{hw}C_p(T6 - T7) \tag{2}$$

where h_g is the outlet enthalpy of the working fluid in the evaporator (kJ/kg); h_e is the inlet enthalpy of the working fluid in the evaporator (kJ/kg); T_6 and T_7 are the inlet and outlet temperatures (in Figure 2) of hot water, respectively (K).

The heat exchange rate in the condenser:

$$Q_{con}^{hp} = \dot{m}_{wf, hp}(h_a - h_d) = \dot{m}_{cw} C_p (T_8 - T_9) \quad (3)$$

where h_a is the inlet enthalpy of the condenser (kJ/kg); h_d is the outlet enthalpy of the condenser (kJ/kg); T_8 and T_9 are the outlet and inlet temperatures (in Figure 2) of the cooling water, respectively (K).

Compressor power:

$$W_{com}^{hp} = \dot{m}_{wf, hp}(h_{as} - h_g) / \eta_{ie} / \eta_{com} \quad (4)$$

where h_{as} is the outlet enthalpy of the compressor in theory (kJ/kg).

The isentropic efficiency of the heat pump compressor changes with operating conditions. Here, an empirical formula, assuming that the isentropic efficiency of the compressor is a function of the pressure ratio [38], is used in our model, as follows:

$$\eta_{ie} = 0.83955 - 0.01026 \left(\frac{P_{as}}{P_g} \right) - 0.00097 \left(\frac{P_{as}}{P_g} \right)^2 \quad (5)$$

where P_{as} is the outlet pressure of the compressor (MPa); P_g is the inlet pressure of the compressor (MPa).

The coefficient of performance of the heat pump is given by

$$COP = Q_{con}^{hp} / W_{com}^{hp} \quad (6)$$

The heat pump is the main power consumption equipment in the system. Its power consumption has a great influence on the techno-economy of the system.

2.1.3. Heat Exchanger

The heat exchanger is important equipment which couples the geothermal cycle and the heating system. Equations (7)–(9) are the basic formulas for the heat exchanger.

$$Q_{tot}^{ex} = \dot{m}_1^{ex} C_p (T_{1,i}^{ex} - T_{1,o}^{ex}) = \dot{m}_2^{ex} C_p (T_{2,o}^{ex} - T_{2,i}^{ex}) \quad (7)$$

$$Q_{tot}^{ex} = k_m^{ex} A_{tot}^{ex} \Delta T_m^{ex} \quad (8)$$

$$\Delta T_m^{ex} = \frac{\Delta T_{max} - \Delta T_{min}}{\ln(\Delta T_{max} / \Delta T_{min})} \quad (9)$$

where \dot{m}_1^{ex} is the mass flow rate of hot water (kg/s); \dot{m}_2^{ex} is the mass flow rate of cooling water (kg/s); k_m^{ex} is the heat transfer coefficient (kW/(m²·K)); A_{tot}^{ex} is the heat transfer area (m²); ΔT_m^{ex} is the logarithmic mean temperature difference (LMTD) (K); ΔT_{max} and ΔT_{min} represent the larger value and the smaller value of the end temperature differences of the heat exchanger, respectively (K).

Equations (7)–(9) are applicable to both Heat Exchanger 1 and Heat Exchanger 2 in Figure 2. In this case, $T_{1,i}^{ex}$ represents T1 for Heat Exchanger 1 or T2 for Heat Exchanger 2. $T_{2,o}^{ex}$ represents T4 for Heat Exchanger 1 or T6 for Heat Exchanger 2.

2.1.4. Energy Storage Tank

The design and selection of the energy storage tank are very important for the optimization of the heating system investigated. The water tank adopted in this paper is a cylinder; the height-to-diameter ratio is 1. It is assumed that the internal temperature of

the water tank is uniform. Taking the water tank as a control volume, the mathematical expression is obtained according to the conservation of energy, as follows:

$$MC_p \frac{dT_\tau}{d\tau} = F_1 \dot{m}_{\tau,st} C_p (T_{\tau,st} - T_\tau) - F_2 \dot{m}_{\tau,he} C_p (T_\tau - T_{\tau,he}) - k_t A_t (T_\tau - T_o(\tau)) / 1000 \quad (10)$$

$$\begin{cases} F_1 = 1, F_2 = 0 & \text{The tank for storage.} \\ F_1 = 0, F_2 = 1 & \text{The tank for heating.} \end{cases} \quad (11)$$

where T_τ is the temperature of the water tank (K); $\dot{m}_{\tau,st}$ is the mass flow rate of the water tank during energy storage (kg/s); $T_{\tau,st}$ is the inlet temperature of the water tank during energy storage (K); $\dot{m}_{\tau,he}$ is the mass flow rate of the water tank during heating (kg/s); $T_{\tau,he}$ is the inlet temperature of the water tank during heating (K); k_t is the overall heat transfer coefficient between the hot water inside the water tank and the surroundings of the water tank, set as 0.2 based on the actual situation (W/(m²·K)); A_t is the surface area of the tank (m²). Equation (11) shows that when the water tank is storing heat, $F_1 = 1$ and $F_2 = 0$. Conversely, when the water tank supplies heat to the building, $F_1 = 0$ and $F_2 = 1$.

2.1.5. Water Pump

The frictional head loss and local head loss in the system are important parts in the water supply calculation. The electric energy input to the water pump is needed to balance those losses. The power consumption of the pump is calculated by

$$W_{wp} = \alpha \dot{m}_{wp} g (H_1 + H_2 + H_3) / \eta_{wp} / 1000 \quad (12)$$

where α is the margin coefficient, set as 1.1 [39]; H_1 is the frictional head loss (m); H_2 is the local head loss when water flows through the equipment, and its value is referred to the relevant specifications (m) [40]; H_3 is the local head loss when water flows through valves and bends (m); η_{wp} is the water pump efficiency which is given by Equation (A1) in Appendix A.

The relationship between the water pump head (H) and pressure loss (ΔP) is as follows:

$$H = \frac{\Delta P}{\rho g} \quad (13)$$

The pressure loss along the path is calculated by Hazen–Williams Formulas (14) and (15):

$$i_u = 105 C_h^{-1.85} d_j^{-4.87} q_g^{1.85} K \quad (14)$$

$$\Delta P_{al} = 1000 i_u L \quad (15)$$

where C_h is the Hazen–Williams coefficient, set as 140 [41]; K is the correction coefficient [41]; ΔP_{al} is the pressure loss along the path (Pa).

The local pressure loss is given by

$$\Delta P_{lo} = \zeta \frac{\rho v^2}{2} \quad (16)$$

where ΔP_{lo} is the local pressure loss (Pa); ζ is the coefficient of local resistance [40].

2.2. Operation Model

2.2.1. Operation Modes

The operation is divided into three stages in a day, corresponding to the following four operation modes:

- Mode 1: energy storage in the water tank;
- Mode 2: water tank heating;
- Mode 3: conventional heating;

Mode 4: no operation.

According to the electricity price in different periods, shifting the modes may achieve better performance in reducing operating cost, while ensuring the heating quality of the office building.

Table 1 shows the time-of-use electricity prices in Xianxian. According to Table 1, the energy storage in the water tank (Mode 1) is selected for the time from 22:00 to 6:00, corresponding to a low electricity price, and its operation system is shown in Figure 5a. In this mode, the heat storage stops when the temperature of the water tank meets its maximum value or the heat storage time meets 8 h. From 8:00 to 20:00 is the stage for building heating, when the electricity price is at peak or flat value, and the operation mode is water tank heating (Mode 2) or conventional heating (Mode 3). The detailed heating strategy is described in Section 2.2.2. The operating systems corresponding to Mode 2 and Mode 3 are shown in Figure 5b,c, respectively. The difference between Mode 3 and Mode 1 is that in Mode 1 the heat is supplied to the water tank instead of to the building.

Table 1. Time-of-use electricity prices of nonresidents in Hebei Southern power grid.

Period of Using Electricity in the Course of a Day	Price Names *
8:00 a.m.–12:00 p.m.; 4:00 p.m.–8:00 p.m.	Peak price
6:00 a.m.–8:00 a.m.; 12:00 p.m.–4:00 p.m.; 8:00 p.m.–10:00 p.m.	Flat price
10:00 p.m.–12:00 a.m.; 12:00 a.m.–6:00 a.m.	Valley price

* Details about the electricity price are shown in Tables 2 and 3.

2.2.2. Operation Strategies

Four operating strategies are proposed in this paper, as shown in Figure 6. These heating strategies differ only in building heating time, and have no difference in the energy storage at night.

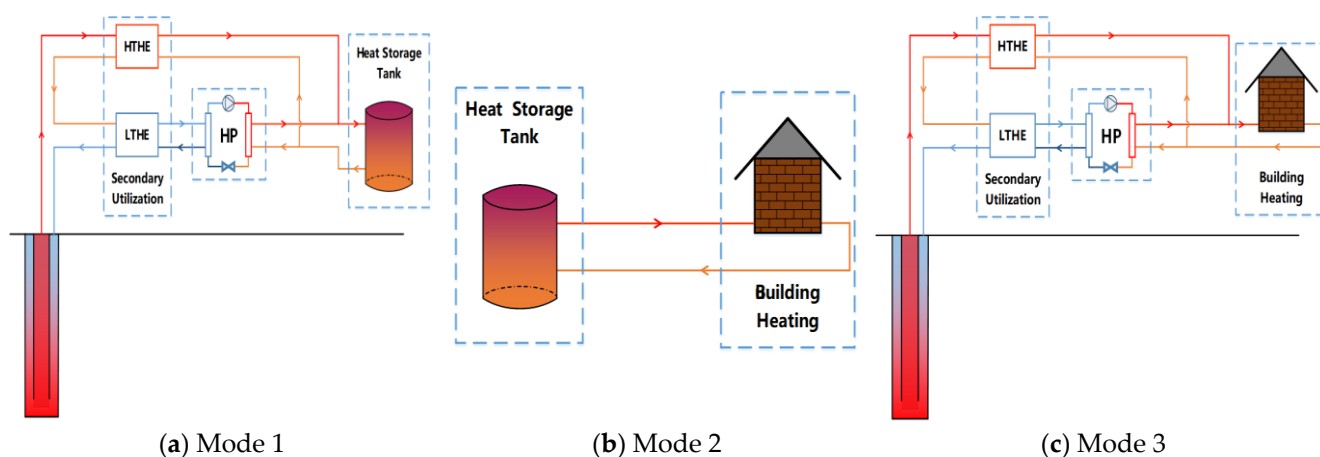


Figure 5. Schematic diagram of three operation modes: (a) water tank heat storage mode (Mode 1); (b) water tank heating mode (Mode 2); (c) conventional heating mode (Mode 3).

Case 1 (Figure 6a) indicates that the water tank heating mode is preferred to be operated during the day. When the temperature of the water tank reaches its lower limit, the heating mode is switched to the conventional heating mode. Case 2 (Figure 6b) indicates that the water tank is preferred for heating during 8:00–12:00 and 16:00–20:00. If it is predicted that the water tank still has available heat after meeting the heat load of these two periods, the water tank heating mode is also preferred for operating in the other period; otherwise, the conventional heating mode is used. This strategy is proposed because of the larger heat load and higher electricity price during 8:00–12:00 and 18:00–20:00. Case 3 (Figure 6c) shows that the water tank heating mode and the conventional heating mode operate at the same time, and the water tank heat is supplied for the peak load (i.e., the

conventional heating mode is used to meet the base load). Contrary to Case 3, Case 4 (Figure 6d) indicates that the conventional heating is used for the peak load (i.e., the water tank heating for the base load). All four strategies need to ensure that the water tank temperature reaches its lower limit at 20:00, unless the heat stored in the tank is higher than the daytime heat load.

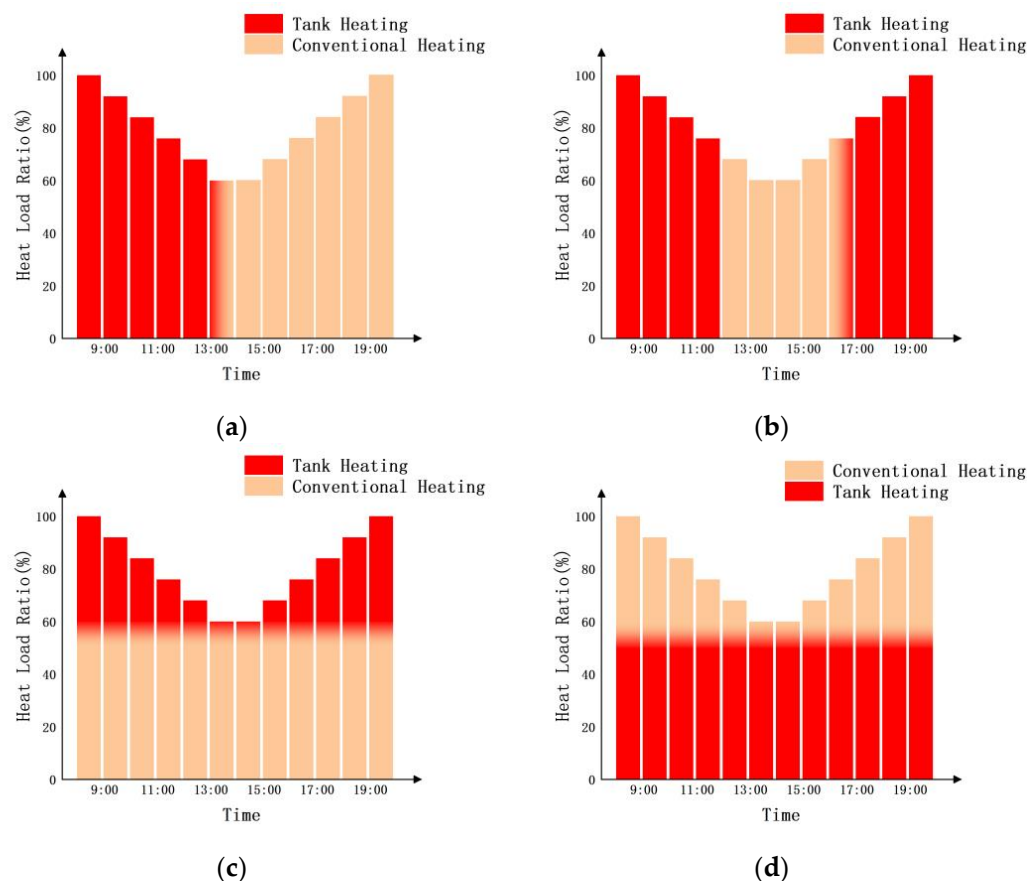


Figure 6. Four operation strategies: (a) Case 1; (b) Case 2; (c) Case 3; (d) Case 4.

Case 1 and Case 2 operate two heating modes alternately, with the corresponding system shown in Figure 2. In Case 3 and Case 4, the water tank heating mode and the conventional heating mode operate simultaneously, so the system can save one water pump, with the corresponding system shown in Figure 7.

2.2.3. Operation Conditions

In the system optimization, the following assumptions have been made:

- (1) The supply water temperature (T_{10}) for conventional heating is same as the average of the upper and lower limit temperatures of the energy storage tank (i.e., to maintain the same quality of heating). The upper limit temperature of the water tank (T_{\max}) is a decision variable which represents the highest temperature that the water tank can reach during heat storage at night. The lower limit temperature of the water tank (T_{\min}) is designed to be 40 °C, corresponding to the lowest temperature that the water tank can reach during daytime heating.
- (2) The outlet temperature of Heat Exchanger 1 (T_2) in the conventional heating mode is the same as the averaged T_2 in the water tank energy storage mode.
- (3) The difference between the inflow and outflow water temperatures for building heating is not more than 8 °C; this is necessary to make sure that the heating water temperature is not low when it reaches the last room.

- (4) The geofluid temperature at the wellhead (T1) is 70 °C; the reinjection geofluid temperature (T3) is in the following range: 13 °C < T3 < 17 °C; T4 = T8 (applies to Figure 2); and T4 = T8 = T12 (applies to Figure 7).

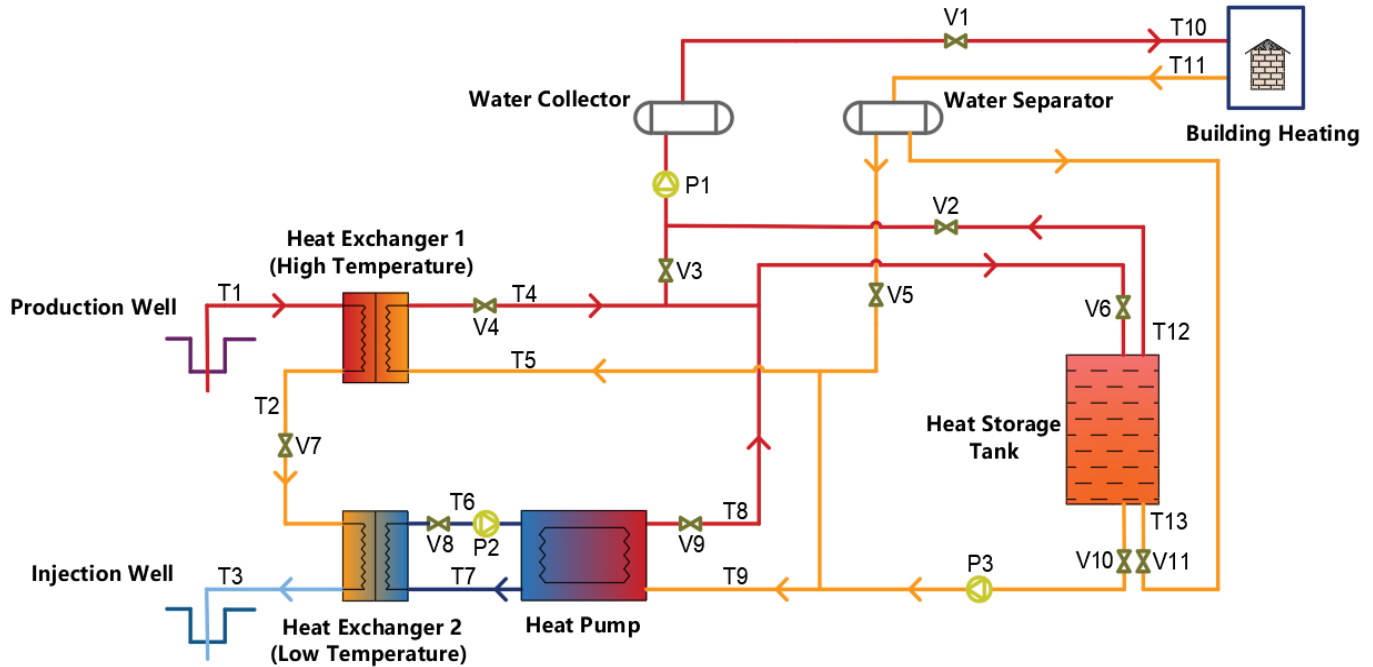


Figure 7. Energy storage–geothermal coupled heating system for Case 3 and Case 4.

2.3. Optimization Model

2.3.1. Decision Variables

In this study, four decision variables (T_{\max} , ϵ , ΔT_e , ΔT_{hp}) were used for the optimization. They, together with their constraints, are described as follows:

- (1) The upper limit temperature of the energy storage tank (T_{\max}): ranging from 46 °C to 55 °C (subject to heating temperature of the heat pump).
- (2) The energy storage ratio (ϵ): ratio of the maximum heat-stored in the energy storage tank to the average daily heating load of the design week, ranging from 0 to 1.
- (3) End temperature difference at low temperature side of the Heat Exchanger 1 ($\Delta T_e = T_2 - T_5$, Figure 2): ranging from: 1 °C to 7 °C (subject to the heat exchanger specification).
- (4) Maximum temperature difference of the heat pump system ($\Delta T_{hp} = T_8 - T_7$, Figure 2): ranging from: 35–40 °C (subject to the heat pump specification).

2.3.2. Objective Function

In this study, levelized cost of heat (LCOH) was used to evaluate the engineering economy of the composite system; the LCOH refers to the cost of obtaining unit heat energy and is similar to the levelized cost of electricity [42,43]. The objective function used in this study is the minimization of the LCOH. The calculation includes two parts. The first part is the ratio of the sum of the annual investment cost and annual maintenance cost to the heat load of the whole heating period (120 days); the second part is the ratio of the operating cost to the heat load of the design week. The objective function is as follows:

$$\min LCOH = \min \left\{ \frac{COST \cdot CRF + C_{main}}{Q'_S} + \frac{OC}{Q'_W} \right\} \quad (17)$$

where Q'_S and Q'_W are heating load of the heating season and the design week, respectively (kJ); $COST$ is the investment cost of the system, including equipment cost and other costs that are calculated at CNY 60 (USD 8.976) per square meter of heating area. OC is the

operating cost of the system. Both of these are functions of the decision variables, as shown below. Detailed formulas of $COST$ and OC are given in Appendix B.

$$COST = f_1(T_{max}, \varepsilon, T_e, T_{hp}) \quad (18)$$

$$OC = f_2(T_{max}, \varepsilon, T_e, T_{hp}) \quad (19)$$

Capital recovery factor (CRF) and annual maintenance cost (C_{main}) are calculated as follows:

$$CRF = \frac{i \cdot (1 + i)^n}{(1 + i)^n - 1} \quad (20)$$

$$C_{main} = \beta \cdot COST \quad (21)$$

where i is the interest rate, set as 5%; n is the service life of the system, set as 25 (a); β is the proportion of annual maintenance cost, set as 1%.

3. Results and Discussion

3.1. Optimal Values of Decision Variables in Different Scenarios

For the system in this study, the investment cost of major equipment and the time-of-use electricity prices are important factors that affect the total cost of the optimization results. Ten scenarios were investigated (as shown in Table 2) according to different equipment prices and time-of-use electricity prices, with the first scenario taken as the basic scenario. Each of the remaining scenarios is obtained by modifying a parameter from the basic scenario. Each region name in Table 2 only represents the time-of-use electricity price of that region, with the corresponding value given in Table 3.

Table 2. Parameters used for optimization under 10 scenarios.

Scenario	Region	Energy Storage Tank Price (CNY/m ³)	Heat Pump Price (CNY/kW)	Heat Exchanger Price (CNY/m ²)	Water Pump Price (CNY/kW)
1 (basic scenario)	Xianxian Region	1000	1000	800	2000
2	-	-	-	2000	-
3	-	-	500	-	-
4	-	-	1500	-	-
5	Shanghai Region	-	-	-	-
6	-	-	-	-	1000
7	-	-	-	-	3000
8	-	500	-	-	-
9	-	1500	-	-	-
10	Tianjin Region	-	-	-	-

"-" means the same as the values in scenario 1 (CNY can be converted into USD based on CNY 1 = USD 0.1496 on 1 June 2022).

Table 3. Time-of-use electricity prices for three regions used in this study (CNY/kW·h).

Time	Status	Xianxian Region	Shanghai Region	Tianjin Region
8:00 a.m.–12:00 p.m.; 4:00 p.m.–8:00 p.m.	High peak	0.9304	1.11	1.2760
12:00 p.m.–4:00 p.m.	Flat stage	0.6724	1.11	0.8305
10:00 p.m.–12:00 a.m.; 12:00 a.m.–6:00 a.m.	Low valley	0.4144	0.527	0.4050

CNY can be converted into USD based on CNY 1 = USD 0.1496 on 1 June 2022.

It is worth noting that in each scenario of Table 2, it is assumed that the same geothermal well (with same geofluid conditions) is used and the heating demand does not change in each scenario.

In this study, all the decision variables in each scenario in Table 2 are optimized based on the objective function (min LCOH), and the optimal decision variables for all the scenarios in each operating strategy are obtained as shown in Figure 8, where the abscissa

represents the 10 scenarios in Table 2. The optimization results of the four decision variables (ϵ , T_{max} , ΔT_e , and ΔT_{hp}) are discussed successively.

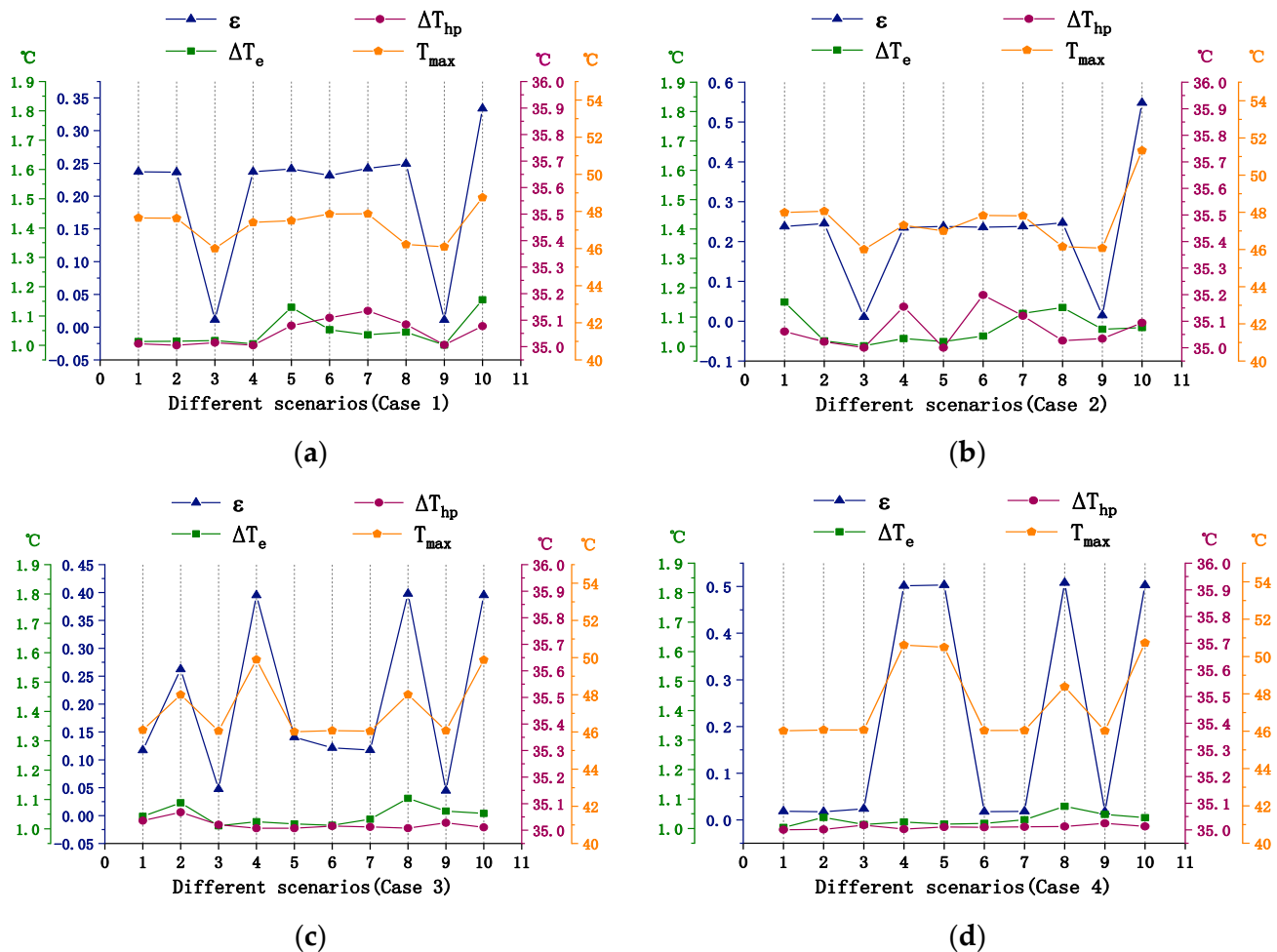


Figure 8. Optimal decision variables for different scenarios under the four strategic conditions: (a) Case 1 (Strategy 1); (b) Case 2 (Strategy 2); (c) Case 3 (Strategy 3); (d) Case 4 (Strategy 4).

The optimal energy storage ratio (ϵ) essentially reflects the optimal energy storage in the system. If the optimal value of the energy storage ratio approaches 0, it indicates that the energy storage device is not suitable to be used in the situation investigated. Therefore, in Case 1 and Case 2, it is not applicable to use the energy storage tank for scenario 3 and scenario 9, but it is applicable to use for all other scenarios. The optimal energy storage ratio is 33% for scenario 10 in Case 1, 55% for scenario 10 in Case 2, and around 24% for all other scenarios in Case 1 and Case 2. In Case 3, the energy storage tank should be used for all scenarios. Among them, the optimal energy storage ratios for scenario 3 and scenario 9 are the lowest, close to 5%. This is because the hot water tank is used for peak load in Case 3, and a small amount of energy storage is enough to reduce the heating load of the heat pump; hence, the investment cost of the heat pump can be reduced. The optimal storage ratios for other scenarios are high in Case 3, around values of 12%, 26%, and 40%. In Case 4, it is applicable to use the energy storage tank in scenarios 4, 5, 8, and 10, with optimal storage ratios around 50%. However, it is not applicable to use the energy storage tank for the remaining scenarios in Case 4.

The upper temperature limit of the energy storage tank (T_{max}) is also an important parameter. For the same amount of energy storage, the lower the T_{max} , the larger the tank size, and the higher the investment cost of the tank. If the T_{max} is high, higher heat pump power is needed to achieve higher outlet temperature, resulting in a higher operating

cost. As can be seen in Figure 8, T_{max} and ϵ show a similar trend. Among them, T_{max} has the highest value for scenario 10 in Case 2, around 51.5 °C. In this situation, the optimal temperature difference of the heat storage ($T_{max}-T_{min} = 51.5-40$) is 11.5 °C. For most of the remaining scenarios in Case 1 and Case 2, the optimal values for T_{max} are around 48 °C, and the optimal temperature difference of the heat storage ($T_{max}-T_{min}$) is 8 °C. In Case 3 and Case 4, no value of T_{max} exceeds 51.5 °C.

ΔT_e and ΔT_{hp} denote the end temperature difference at the low-temperature side of Heat Exchanger 1 and the maximum temperature difference of the heat pump system, respectively. If the values of ΔT_e and ΔT_{hp} are reduced, the operating cost of the system will be reduced, but the investment cost will be increased. In all scenarios shown in Figure 8, no matter which strategy is used, the optimal values of ΔT_e and ΔT_{hp} are both within the constraint range.

3.2. Minimum LCOH of each Scenario

The minimum LCOH is obtained for each scenario, as shown by the red bar in Figure 9. In addition, the blue bar represents the minimum LCOH of the system without using the energy storage tank in that scenario. Each line in the line chart shows the reduction percentage of the minimum LCOH obtained by comparing the system using an energy storage tank and that not using a tank.

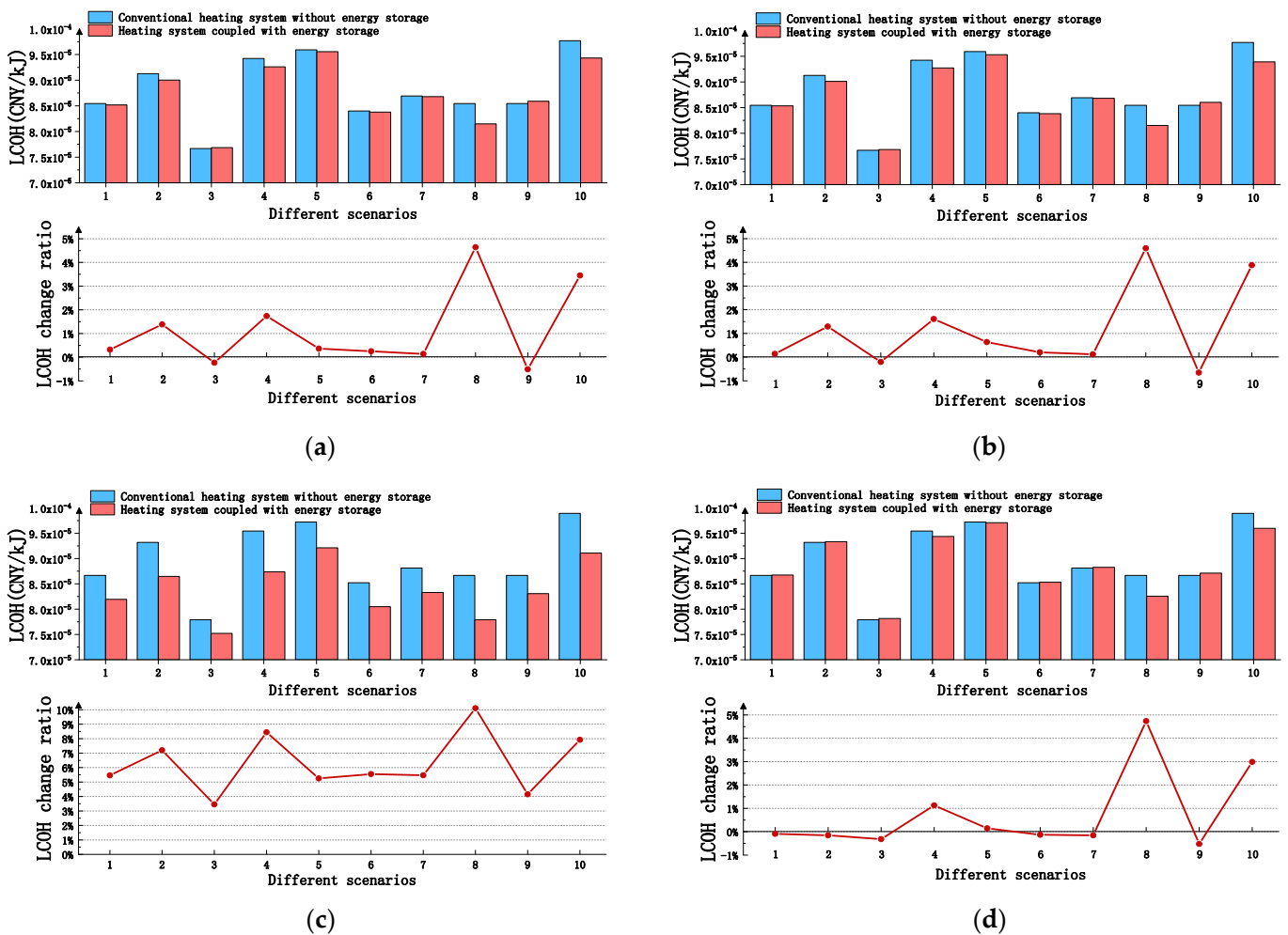


Figure 9. Minimum LCOH of each scenario: comparison between the conventional heating system and the heating system coupled with energy storage: (a) Case 1; (b) Case 2; (c) Case 3; (d) Case 4. CNY can be converted into USD based on CNY 1 = USD 0.1496 on 1 June 2022.

Figure 9 shows that in Case 1 and Case 2, more than 1% LCOH can be saved in scenarios 2, 4, 8, and 10 under the conditions that the heating systems are coupled with energy storage. Among them, scenario 8 has the largest saving proportion, which exceeds 4.5% in each strategy. Case 3 shows a relatively high saving proportion for most of the scenarios, with the lowest percentage reaching about 3.5% and the highest reaching as high as 10%. In Case 4, scenario 8 also has the highest saving proportion, with a value of 4.7%, and scenarios 4 and 10 also show good saving percentages that exceed 1%. Each of the saving ratios with a negative value in Figure 9a,b,d indicate that it is not applicable to use an energy storage tank in the heating system.

Figure 10 shows the comparison of the minimum LCOHs among the four operation strategies. It can be seen that the red line (Case 1) and the black line (Case 2) are almost identical. The LCOHs in Case 3 are less than those in other Cases for each scenario. Especially in scenario 4, the LCOH in Case 3 is about 7.4% lower than that in Case 4, and 5.7% lower than that in Case 1 and Case 2. This is because the use of the water tank can effectively reduce the investment cost of other equipment when the energy storage device is used for the peak load. It can also be seen that Case 4 has the highest LCOHs for all scenarios, indicating that this operating strategy is not a good choice. The LCOH values of Case 1 and Case 2 are relatively moderate, and the difference between the total costs in the two cases can be negligible, but in terms of operational simplicity, Case 1 is better.

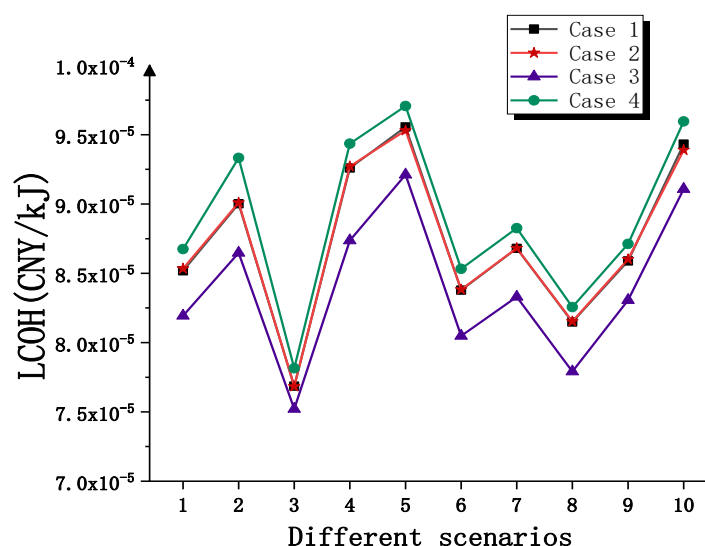


Figure 10. Comparison of minimum LCOHs among the four operation strategies (CNY can be converted into USD based on CNY 1 = USD 0.1496 on 1 June 2022).

3.3. Sensitivity Analysis

3.3.1. The Influence of Energy Storage Ratio on Operating Cost

In order to find the relationship between operating cost and energy storage ratio, the basic scenario (in Table 2) is selected for study in this section. Each strategy is optimized, taking min LCOH as the objective function, based on which the optimal values of the four decision variables are obtained. The optimal values of T_{max} , ΔT_e , and ΔT_{hp} are used for analyzing the influence of energy storage ratio (ϵ) on the total operating cost during the design week, as shown in Figure 11.

It can be seen from Figure 11 that the operating cost of the system is significantly reduced in each strategy as the energy storage ratio increases, but the minimum operating cost and the reduction trend with the increase of the energy storage ratio are different from case to case. In Case 1, the operating cost shows a rapid decline as the energy storage ratio increases until it reaches 0.4, the operating cost then levels off from 0.4 to 0.7, then it drops again when the energy storage ratio increases from 0.7 to 1. This is due to the higher electricity price and larger heat load in the morning and evening. The curves corresponding

to Case 3 and Case 4 show monotonic declines, but the operating cost in Case 3 is lower than that in Case 4. For the three operating strategies (cases 1, 3, and 4), the lowest operating cost in each case corresponds to a value of energy storage ratio of 1, with the lowest values of operating costs being CNY 264.6 (USD 39.58), CNY 258 (USD 38.60), and CNY 263 (USD 39.34), respectively. The Case 2 curve shows a decline first and then an uptrend after the energy storage ratio is greater than 0.74, corresponding to an operating cost of CNY 255.13 (USD 38.17), which is the lowest cost among the four cases. Compared with the system without using the energy storage tank ($\epsilon = 0$), the operating cost in Case 2 can be reduced to about 30%.

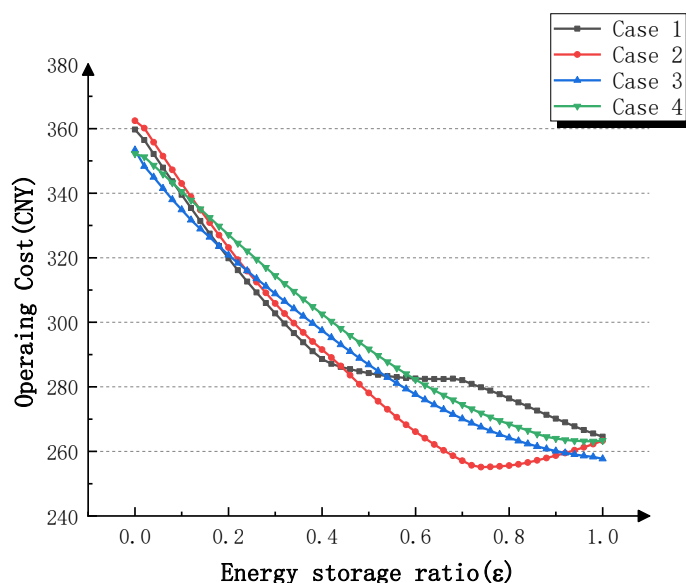


Figure 11. The influence of energy storage ratio on operating cost (CNY can be converted into USD based on CNY 1 = USD 0.1496 on 1 June 2022).

3.3.2. The Influence of Electricity Price and Tank Price on ϵ_0 and LCOH

The peak and valley electricity prices, as well as the water tank price, are important parameters that influence the optimal energy storage ratio (ϵ_0) and LCOH of the system. Therefore, sensitivity analysis was carried out and the results are shown in Figure 12. The dashed lines (red and black) represent the influence of electricity price on ϵ_0 (shown by the right vertical axis) and LCOH (shown by the left vertical axis), respectively. The solid lines (red and black) represent the influence of the energy storage tank price on ϵ_0 and LCOH, respectively.

The actual values represented by the numbers on the horizontal axis are shown in Table 4. The number 0 represents the basic scenario (shown in Table 2), corresponding to the energy storage tank price of CNY 1000/m³ (USD 149.6/m³) and the peak-valley electricity price difference of CNY 0.516/kW·h (USD 0.0772/kW·h).

The influences of the peak-valley electricity price difference and the tank price on the optimal energy storage ratio (ϵ_0) are shown by the two red lines (dashed and solid, respectively) in Figure 12. In Case 1 (Figure 12a) and Case 2 (Figure 12b), when the peak-valley price difference is higher than CNY 0.466/kW·h (USD 0.0697/kW·h), i.e., for the scenarios with abscissa number greater than or equal to 0, the optimal energy storage ratios are greater than 0.23 (see red dashed lines, Figure 12a,b), which means it is applicable to use the energy storage tank under this condition. Similarly, when the energy storage tank price is lower than CNY 1100/m³ (USD 164.56/m³), i.e., for the scenarios with abscissa number less than or equal to 0, it is also applicable to use the energy storage tank (see red solid lines, Figure 12a,b). In Case 3 (Figure 12c), an energy storage tank can be used for any scenario; in other words, there is no other choice but to use an energy storage tank in Case 3. In Figure 12d (Case 4), it is suitable to use an energy storage tank in the heating system when

the peak-valley price difference is greater than CNY 0.566/kW·h (USD 0.0847/kW·h) for the scenarios with abscissa number greater than or equal to 2, or when the energy storage tank price is lower than CNY 900/m³ (USD 134.64/m³) for the scenarios with abscissa number less than or equal to -2.

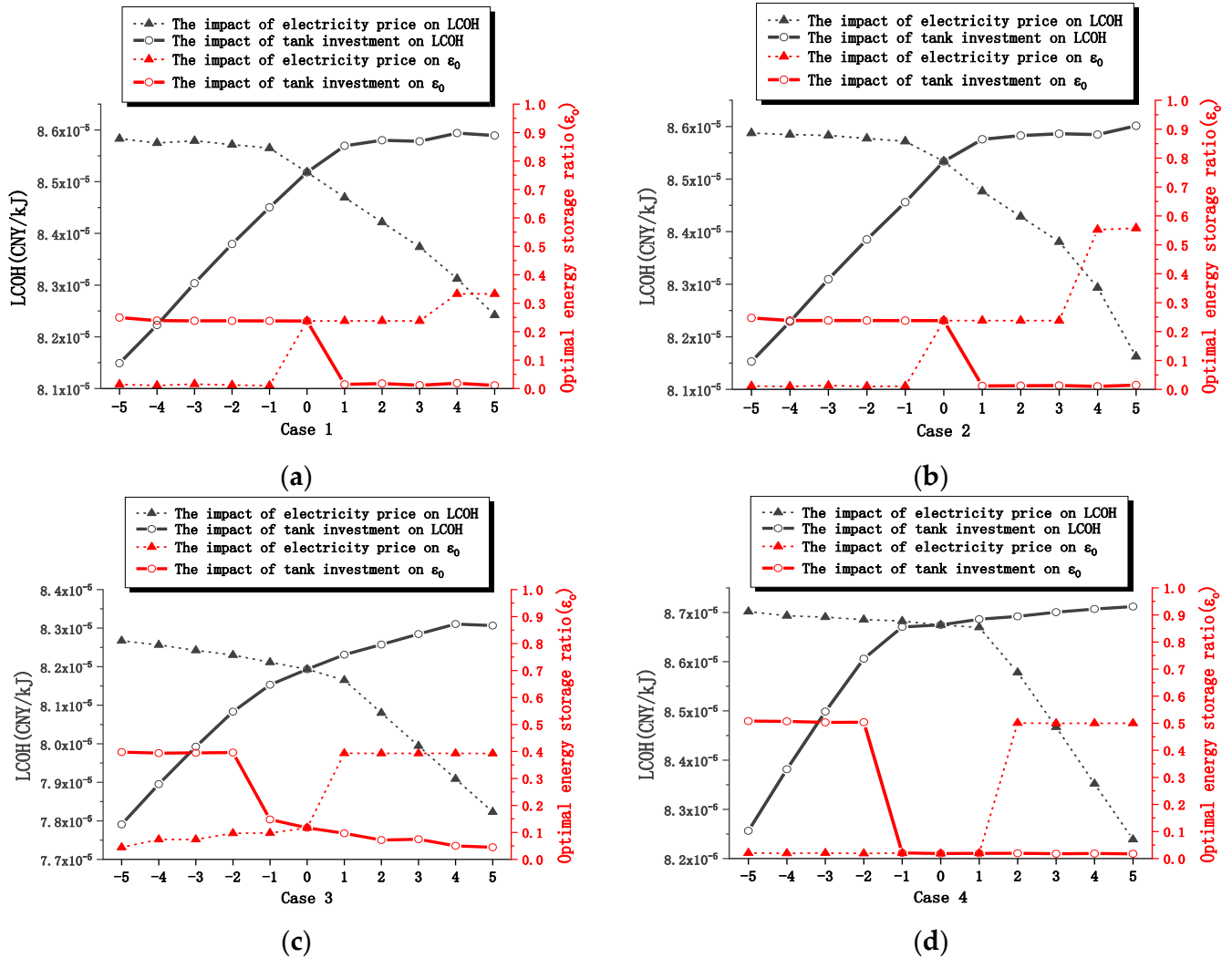


Figure 12. Sensitivity analysis by adjusting the energy storage tank price and peak-valley electricity price difference: (a) Case 1; (b) Case 2; (c) Case 3; (d) Case 4. CNY can be converted into USD based on CNY 1 = USD 0.1496 on 1 June 2022.

Table 4. The actual values represented by the numbers on the horizontal axis in Figure 12.

Abscissa	-5	-4	-3	-2	-1	0	1	2	3	4	5
The peak-valley electricity price difference (CNY/kW·h)	0.266	0.316	0.366	0.416	0.466	0.516	0.566	0.616	0.666	0.716	0.766
Energy storage tank price (CNY/m ³)	500	600	700	800	900	1000	1100	1200	1300	1400	1500

CNY can be converted into USD based on CNY 1 = USD 0.1496 on 1 June 2022.

The Influences of the peak-valley electricity price difference and the tank price on the LCOHs are shown by the two black lines (dashed and solid, respectively) in Figure 12. As can be seen from Figure 12, the LCOHs become sensitive to the two prices under the following conditions: in Case 1 and Case 2, the electricity price difference should be greater than CNY 0.466/kW·h (USD 0.0697/kW·h) or the tank price should be less than CNY

1100/m³ (USD 164.56/m³); while in Case 3 and Case 4, the electricity price difference should be greater than CNY 0.566/kW·h (USD 0.0847/kW·h) or the tank price should be less than CNY 900/m³ (USD 134.64/m³), respectively. These results indicate that Case 3 and Case 4 have less applicable scope of using an energy storage tank than Case 1 and Case 2.

4. Conclusions

The purpose of this study is to find the optimal operation strategy and optimal design parameters of an energy storage–geothermal coupled heating system for office building heating. Four heating operation strategies are proposed according to the characteristics of the building’s heat load and time-of-use electricity prices. In addition, 10 scenarios are proposed considering different equipment prices and time-of-use electricity prices in different regions of China. Optimization of the coupled heating system was carried out using minimization of LCOH as the objective function. The main conclusions are as follows:

- (1) The four operating strategies show that coupling an energy storage tank to the geothermal heating system can reduce operating costs by more than 25%. Case 2 is the best among the four operating strategies, and can reduce operating costs by 30% when the energy storage ratio is 74%.
- (2) When the system design is optimized in the consideration of both operating costs and investment costs, the operation strategy (Case 3) where the energy storage tank is used for supplying the peak heat load has a lower LCOH than other cases. The operation strategy (Case 4) where the energy storage tank is used to meet the basic heat load has the worst performance.
- (3) It is applicable to couple an energy storage tank to the heating system in scenarios 4, 8, and 10. In scenario 8, the coupled system can save up to 10% LCOH compared with the system without using an energy storage tank. It is worth noting that none of the optimal storage ratios exceed 55% for all scenarios.
- (4) The sensitivity analysis shows that coupling an energy storage tank to a geothermal heating system can reduce LCOH when peak-valley electricity price difference is higher than CNY 0.566/kW·h (USD 0.0847/kW·h) or the tank price is lower than CNY 900/m³ (USD 134.64/m³); otherwise, the techno-economy may not be good.
- (5) The results obtained in this study provide a reference for the design of an energy storage–geothermal coupled heating system. In the near future, an experimental study will be carried out to further validate the model, as well as the results obtained here.

Author Contributions: Conceptualization, Y.R., X.L. and W.Z.; data curation, J.Z., J.L., Z.C., T.Z. and Y.Z.; formal analysis, Y.R., X.L., W.Z., J.Z. and H.Y.; funding acquisition, X.L.; investigation, W.Z., J.Z., J.L., F.M. and H.Y.; methodology, Y.R., X.L., W.Z. and Z.C.; project administration, X.L. and F.M.; software, Y.R.; supervision, X.L.; writing—original draft, Y.R.; writing—review and editing, X.L., J.Z., J.L., T.Z. and Y.Z. All authors have read and agreed to the published version of the manuscript.

Funding: This research was funded by “Ministry of Science and Technology: 2019YFB1504105”.

Institutional Review Board Statement: Not applicable.

Informed Consent Statement: Not applicable.

Data Availability Statement: Not applicable.

Acknowledgments: The authors gratefully acknowledge the financial support provided by the National Key Research and Development Program of the 13th Five-Year Plan of China (No. 2019YFB1504105).

Conflicts of Interest: The authors declare no conflict of interest.

Nomenclature

Roma symbols

A	Area
C_h	Hazen–Williams coefficient
C_{main}	Annual maintenance cost
C_p	Specific heat at constant pressure
d_j	Inside diameter
g	Gravitational acceleration
H	Head loss
h	Enthalpy
i	Interest rate
i_u	Pressure loss per unit length
K	Correction coefficient
k	Heat transfer coefficient
L	Length
M	Mass
\dot{m}	Mass flow rate
n	Service life of the system
P	Pressure
$P1, P2, \dots$	Pump
Q	Heat transfer rate
Q'	Heat
q_g	Volume flowrate
T	Temperature
V	Volume
$V1, V2, \dots$	Valve
W	Power

Greek symbols

α	Margin coefficient
β	Proportion of annual maintenance cost
ε	Energy storage ratio
ε_o	Optimal energy storage ratio
η	Efficiency
λ	Ratio of mass flow rate
ζ	Coefficient of local resistance
ρ	Density of water
τ	Time
v	Flow velocity

Subscripts

al	Along
B	Building
com	Compressor
con	Condenser
cw	Cooling water
d	Design
e	Heat exchanger
ele	Electricity
eva	Evaporator
he	Heating
hp	Heat pump
hw	Hot water
i	In
ie	Isentropic
lo	Local
m	Mean
max	Maximum

<i>min</i>	Minimum
<i>o</i>	Out
<i>S</i>	Season
<i>st</i>	Storage
<i>t</i>	Tank
<i>tot</i>	Total
<i>W</i>	Weak
<i>wf</i>	Working fluid
<i>wp</i>	Water pump
Superscripts	
<i>ex</i>	Heat exchanger
<i>hp</i>	Heat pump
Acronyms	
COP	Coefficient of performance
COST	Cost
CPF	Capital recovery factor
GSHP	Ground source heat pump
HVAC	Heating, ventilation, and air conditioning
LCOH	Levelized cost of heat
MD-GHP	Medium and deep geothermal heat pump
OC	Operating cost
PR	Price
TES	Thermal energy storage

Appendix A. Water Pump Efficiency Model

In order to characterize the pump efficiency characteristics, the relationship between water pump efficiency (η_{wp}) and the mass flow ratio was fitted according to the data of the performance of the 12Sh-6 centrifugal pump [44].

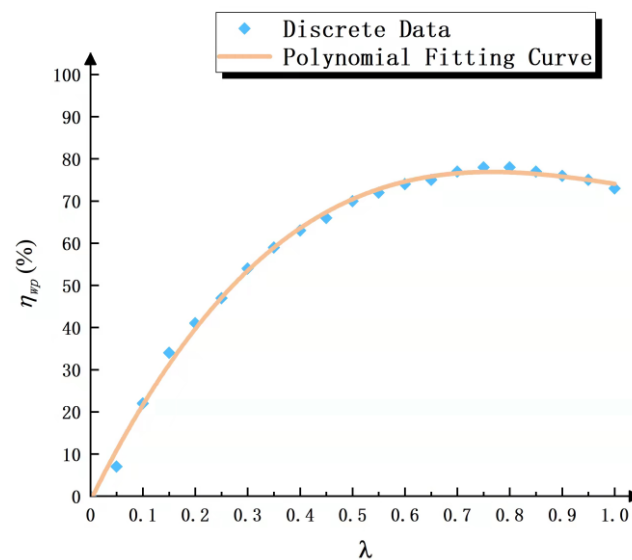


Figure A1. The relationship between water pump efficiency and the ratio of mass flow rate.

The polynomial fitting curve function is as follows:

$$\eta_{wp} = 0.8267\lambda^3 - 2.597\lambda^2 + 2.5215\lambda - 0.0105 \quad (\text{A1})$$

where λ is the ratio of the actual mass flow rate to the maximum mass flow rate.

Appendix B. Investment Cost (COST) and Operating Cost (OC)

The calculation formulas of investment cost (COST) and operating cost (OC) in this study are as follows:

$$COST = COST_{hp} + \sum_{l=1}^2 COST_{e,l} + COST_t + \sum_{n=1}^4 COST_{wp,n} + COST_{other} \quad (A2)$$

where $COST_{hp}$, $COST_{e,l}$, $COST_t$, and $COST_{wp,n}$ are the investment costs of heat pump, heat exchanger, water tank, and water pump, respectively; $COST_{other}$ is other investment cost, including pipeline, valve, and other components, calculated as CNY 60/m² (USD 8.976/m²). l indicates the number of heat exchangers, and n indicates the number of water pumps.

$$COST_{hp} = Q_{hp,d} \times PR_{hp} \quad (A3)$$

where $Q_{hp,d}$ is the design power of the heat pump (kW); PR_{hp} is the unit price of heat pump (CNY/kW).

$$COST_e = A_{e,d} \times PR_e \quad (A4)$$

where $A_{e,d}$ is the design area of the heat exchanger (m²); PR_e is the unit price of heat exchanger (CNY/m²).

$$COST_t = V_{t,d} \times PR_t \quad (A5)$$

where $V_{t,d}$ is the design volume of the water tank (m³); PR_t is the unit price of the water tank (CNY/m³).

$$COST_{wp} = W_{wp,d} \times PR_{wp} \quad (A6)$$

where $W_{wp,d}$ is the design power of the water pump (kW); PR_{wp} is the unit price of water pump (CNY/kW).

$$OC = \sum_{q=1}^{168} \left[\left(W_{hp,q} + \sum_{n=1}^4 W_{wp,n,q} \right) \times PR_{ele,q} \right] \quad (A7)$$

where $W_{hp,q}$ and $W_{wp,n,q}$ are the hourly power consumptions of heat pump and water pump, respectively (kW·h); $PR_{ele,q}$ is the time-of-use electricity price (CNY/kW·h). q indicates the number of operation hours. In this study, the OC is calculated for a period of a design week (168 h).

References

1. Perez-Lombard, L.; Ortiz, J.; Maestre, I.R. The map of energy flow in HVAC systems. *Appl. Energy* **2011**, *88*, 5020–5031. [\[CrossRef\]](#)
2. Efficiency, C. China Building Energy Consumption Annual Report 2020. *Build. Energy Effic.* **2021**, *49*, 1–6.
3. Zhao, J.; Zhu, N.; Wu, Y. The analysis of energy consumption of a commercial building in Tianjin, China. *Energy Policy* **2009**, *37*, 2092–2097. [\[CrossRef\]](#)
4. Shortall, R.; Davidsdottir, B.; Axelsson, G. Geothermal energy for sustainable development: A review of sustainability impacts and assessment frameworks. *Renew. Sustain. Energy Rev.* **2015**, *44*, 391–406. [\[CrossRef\]](#)
5. Self, S.J.; Reddy, B.V.; Rosen, M.A. Geothermal heat pump systems: Status review and comparison with other heating options. *Appl. Energy* **2013**, *101*, 341–348. [\[CrossRef\]](#)
6. Østergaard, P.A.; Lund, H. A renewable energy system in Frederikshavn using low-temperature geothermal energy for district heating. *Appl. Energy* **2011**, *88*, 479–487. [\[CrossRef\]](#)
7. Aghahosseini, A.; Breyer, C. From hot rock to useful energy: A global estimate of enhanced geothermal systems potential. *Appl. Energy* **2020**, *279*, 115769. [\[CrossRef\]](#)
8. Xia, Z.H.; Jia, G.S.; Ma, Z.D.; Wang, J.W.; Zhang, Y.P.; Jin, L.W. Analysis of economy, thermal efficiency and environmental impact of geothermal heating system based on life cycle assessments. *Appl. Energy* **2021**, *303*, 117671. [\[CrossRef\]](#)
9. GB 55010-2021; Projectcode for Heating Engineering. China Architecture & Building Press: Beijing, China, 2021.
10. Huo, Y.L.; Cheng, Y.D.; Li, Y.j.; Jia, J.; Du, Z.Y. Simulation Analysis of Influence of Air Source Heat Pump System on Power Grid Load in Background of Coal-to-Electricity Reform. *J. Huaqiao Univ. (Nat. Sci.)* **2019**, *40*, 756–762.
11. Baeten, B.; Rogiers, F.; Helsen, L. Reduction of heat pump induced peak electricity use and required generation capacity through thermal energy storage and demand response. *Appl. Energy* **2017**, *195*, 184–195. [\[CrossRef\]](#)

12. Han, J.; Cui, M.; Chen, J.; Lv, W. Analysis of thermal performance and economy of ground source heat pump system: A case study of the large building. *Geothermics* **2021**, *89*, 101929. [[CrossRef](#)]
13. Smith, M.; Bevacqua, A.; Tembe, S.; Lal, P. Life cycle analysis (LCA) of residential ground source heat pump systems: A comparative analysis of energy efficiency in New Jersey. *Sustain. Energy Technol. Assess.* **2021**, *47*, 101364. [[CrossRef](#)]
14. Steve, K.; Mike, G.; Kirk, M. Long-Term Commercial GSHP Performance-Part 4: Installation Costs. *ASHRAE J.* **2012**, *54*, 26–36.
15. Deng, Y.; Feng, Z.; Fang, J.; Cao, S.J. Impact of ventilation rates on indoor thermal comfort and energy efficiency of ground-source heat pump system. *Sustain. Cities Soc.* **2018**, *37*, 154–163. [[CrossRef](#)]
16. Urchueguía, J.F.; Zacarés, M.; Corberán, J.M.; Montero, Á.; Martos, J.; Witte, H. Comparison between the energy performance of a ground coupled water to water heat pump system and an air to water heat pump system for heating and cooling in typical conditions of the European Mediterranean coast. *Energy Convers. Manag.* **2008**, *49*, 2917–2923. [[CrossRef](#)]
17. Spitler, J.D.; Gehlin, S. Measured Performance of a Mixed-Use Commercial-Building Ground Source Heat Pump System in Sweden. *Energies* **2019**, *12*, 2020. [[CrossRef](#)]
18. Michopoulos, A.; Bozis, D.; Kikidis, P.; Papakostas, K.; Kyriakis, N.A. Three-years operation experience of a ground source heat pump system in Northern Greece. *Energy Build.* **2007**, *39*, 328–334. [[CrossRef](#)]
19. Michopoulos, A.; Martinopoulos, G.; Papakostas, K.; Kyriakis, N. Energy consumption of a residential building: Comparison of conventional and RES-based systems. *Int. J. Sustain. Energy* **2009**, *28*, 19–27. [[CrossRef](#)]
20. Xu, H.; Lin, L.Q.; Tan, Z.F. Ground Source Heat Pump's Life-cycle Energy Conservation and Technical Economy Analysis Models with Their Application. *Oper. Res. Manag. Sci.* **2018**, *27*, 159–167.
21. Younes, N.; Reza, S.; Mohammad, M.; Ali, A.; Mehdi, H. The effects of ground heat exchanger parameters changes on geothermal heat pump performance—A review. *Appl. Therm. Eng.* **2018**, *129*, 1645–1658.
22. Martinopoulos, G.; Papakostas, K.; Papadopoulos, A. A comparative review of heating systems in EU countries, based on efficiency and fuel cost. *Renew. Sustain. Energy Rev.* **2018**, *90*, 687–699. [[CrossRef](#)]
23. D'Agostino, D.; Greco, A.; Masselli, C.; Minichiello, F. The employment of an earth-to-air heat exchanger as pre-treating unit of an air conditioning system for energy saving: A comparison among different worldwide climatic zones. *Energy Build.* **2020**, *229*, 110517. [[CrossRef](#)] [[PubMed](#)]
24. D'Agostino, D.; Esposito, F.; Greco, A.; Masselli, C.; Minichiello, F. The Energy Performances of a Ground-to-Air Heat Exchanger: A Comparison Among Köppen Climatic Areas. *Energies* **2020**, *13*, 2895. [[CrossRef](#)]
25. D'Agostino, D.; Esposito, F.; Greco, A.; Masselli, C.; Minichiello, F. Parametric Analysis on an Earth-to-Air Heat Exchanger Employed in an Air Conditioning System. *Energies* **2020**, *13*, 2925. [[CrossRef](#)]
26. Zhang, X. Numerical study of geothermal district heating from a ground heat exchanger coupled with a heat pump system. *Appl. Therm. Eng.* **2021**, *185*, 116335. [[CrossRef](#)]
27. Jung, W.; Kim, D.; Kang, B.H.; Chang, Y.S. Investigation of Heat Pump Operation Strategies with Thermal Storage in Heating Conditions. *Energies* **2017**, *10*, 2020. [[CrossRef](#)]
28. Floss, A.; Hofmann, S. Optimized integration of storage tanks in heat pump systems and adapted control strategies. *Energy Build.* **2015**, *100*, 10–15. [[CrossRef](#)]
29. Glembin, J.; Büttner, C.; Steinweg, J.; Rockendorf, G. Thermal Storage Tanks in High Efficiency Heat Pump Systems—Optimized Installation and Operation Parameters. *Energy Procedia* **2015**, *73*, 331–340. [[CrossRef](#)]
30. Lv, J.; Wei, Z.; Zhang, J. Running and economy performance analysis of ground source heat pump with thermal energy storage devices. *Energy Build.* **2016**, *127*, 1108–1116. [[CrossRef](#)]
31. Qi, Y.S.; Yue, Y.L.; Liu, T.Y.; Yuan, D.L. Application analysis of combined ground source heat pump and water energy storage systems. *HV&AC* **2010**, *40*, 94–97.
32. Shah, N.N.; Wilson, C.; Huang, M.J.; Hewitt, N.J. Analysis on field trial of high temperature heat pump integrated with thermal energy storage in domestic retrofit installation. *Appl. Therm. Eng.* **2018**, *143*, 650–659. [[CrossRef](#)]
33. He, P.; Sun, G.; Wang, F.; Wu, H.X. *Heating Engineering*, 4th ed.; China Architecture & Building Press: Beijing, China, 2009; pp. 10–17.
34. Ma, Z.L.; Yao, Y. *Air Conditioning Design for Civil Buildings*, 2nd ed.; Chemical Industry Press: Beijing, China, 2009; pp. 18, 61.
35. China Meteorological Data Service Centre. Available online: <http://data.cma.cn/data/detail/dataCode/A.0012.0001.html> (accessed on 15 March 2021).
36. Cox, G.; Belding, S.; Lowder, T. Application of a novel heat pump model for estimating economic viability and barriers of heat pumps in dairy applications in the United States. *Appl. Energy* **2022**, *310*, 118499. [[CrossRef](#)]
37. Lu, X.; Zhao, Y.; Zhu, J.; Zhang, W. Optimization and applicability of compound power cycles for enhanced geothermal systems. *Appl. Energy* **2018**, *229*, 128–141. [[CrossRef](#)]
38. Dai, B.M.; Liu, S.C.; Li, H.L.; Sun, Z.L.; Song, M.J.; Yang, Q.R. Energetic performance of transcritical CO₂ refrigeration cycles with mechanical subcooling using zeotropic mixture as refrigerant. *Energy* **2018**, *150*, 205–221. [[CrossRef](#)]
39. Zhang, X.K. Study on the Solar and Ground Coupled Heat Pump Heating System. Master's Thesis, Shandong University, Jinan, China, April 2014.
40. Lu, Y.Q. *Practical Heating and Air Conditioning Design Manual*, 2nd ed.; China Architecture & Building Press: Beijing, China, 2007; pp. 1989–1994.
41. Yi, T. The problem of the value of the Hazen-Williams coefficient. *Ind. Water Wastewater* **2004**, *35*, 63–65.

-
42. Astolfi, M.; Xodo, L.; Romano, M.C.; Macchi, E. Technical and economical analysis of a solar–geothermal hybrid plant based on an Organic Rankine Cycle. *Geothermics* **2011**, *40*, 58–68. [[CrossRef](#)]
 43. Walraven, D.; Laenen, B.; D’haeseleer, W. Minimizing the levelized cost of electricity production from low-temperature geothermal heat sources with ORCs: Water or air cooled? *Appl. Energy* **2015**, *142*, 144–153. [[CrossRef](#)]
 44. Baidu Library. Available online: <https://eduai.baidu.com/view/a6af889484868762caaed5f6> (accessed on 10 May 2021).